Complete analysis of spin structure function g_1 of ^{3}He

F. Bissey,[1,2,*] V. Guzey,[1,†] M. Strikman,[3,‡] and A. Thomas[1,§]

[1] *Special Research Centre for the Subatomic Structure of Matter (CSSM) and Department of Physics and Mathematical Physics, Adelaide University, Adelaide 5005, Australia*

[2] *Laboratoire de Physique Corpusculaire, Université Blaise Pascal, CNRS/IN2P3, 24 avenue des Landais, F-63177 Aubière Cedex, France*

[3] *Department of Physics, The Pennsylvania State University, University Park, Pennsylvania 16802*

(Received 8 February 2002; published 6 June 2002)

We present a comprehensive analysis of the nuclear effects important in deep inelastic scattering on polarized ^{3}He over a wide range of Bjorken x, $10^{-4} \leqslant x \leqslant 0.8$. Effects relevant for the extraction of the neutron spin structure function g_1^n from the ^{3}He data are emphasized.

DOI: 10.1103/PhysRevC.65.064317 PACS number(s): 13.60.Hb, 21.45.+v, 24.85.+p, 25.30.−c

I. INTRODUCTION

One of the fundamental challenges of particle physics is to understand the spin structure of protons, neutrons, and nuclei in terms of their quarks and gluons. The main experimental tool, which is hoped to help answer the question, is deep inelastic scattering (DIS) of polarized leptons on polarized targets.

The present work is concerned with the spin structure functions $g_1^{^3\mathrm{He}}$ of the ^{3}He nucleus and g_1^n of the neutron. Since free neutron targets are not available, polarized deuterium and ^{3}He are used as sources of polarized neutrons. The SMC experiments at CERN [1] and the E143 [2] and E155 [3] experiments at SLAC employed polarized deuterium. Polarized ^{3}He was used by the HERMES Collaboration at DESY [4] and the E154 experiment at SLAC [5].

Properties of protons and neutrons embedded in nuclei are expected to be different from those in free space. In particular, the neutron spin structure function g_1^n is not equal to the ^{3}He spin structure function $g_1^{^3\mathrm{He}}$ because of a variety of nuclear effects. These effects include spin depolarization, nuclear binding and Fermi motion of nucleons, the off-shellness of the nucleons, presence of non-nucleonic degrees of freedom, and nuclear shadowing and antishadowing. While each of the above mentioned effects were considered in detail in the literature, no attempt was made to present a coherent and complete picture of all of them in the entire range of Bjorken x. The aim of this work is to combine all the known results for the ^{3}He structure function $g_1^{^3\mathrm{He}}$ in the range $10^{-4} \leqslant x \leqslant 0.8$ and to assess the importance of the nuclear effects on the extraction of the neutron structure function g_1^n from the ^{3}He data.

II. SPIN DEPOLARIZATION, NUCLEAR BINDING, AND FERMI MOTION

The nuclear effects of spin depolarization, binding, and Fermi motion are traditionally described within the framework of the convolution approach [6]. In this approximation, nuclear structure functions are given by the convolution of, in general, the off-shell nucleon structure functions with the light-cone nucleon momentum distributions. As a starting point, we assume that the structure functions of the struck nucleon are those of the free and on-mass-shell nucleon and that non-nucleonic degrees of freedom, such as vector mesons and the Δ isobar, do not contribute. In the following section we shall relax these assumptions. The spin-dependent momentum distributions are given by the probability to find a nucleon with a given light-cone momentum fraction of the nucleus and the helicity of the nucleon aligned along the helicity of the nucleus minus the probability that the helicities of the nucleon and the nucleus are opposite. In general, there is no unique procedure to obtain the light-cone nucleon momentum distributions from the nonrelativistic nuclear wave function. In what follows, we adopt the frequently used convention that the light-cone nucleon momentum distribution can be obtained from the nuclear spectral function [7–9]. Thus $g_1^{^3\mathrm{He}}$ can be represented as the convolution of the neutron (g_1^n) and proton (g_1^p) spin structure functions with the spin-dependent nucleon light-cone momentum distributions $\Delta f_{N/^3\mathrm{He}}(y)$, where y is the ratio of the struck nucleon to nucleus light-cone plus components of the momenta

$$g_1^{^3\mathrm{He}}(x,Q^2) = \int_x^3 \frac{dy}{y} \Delta f_{n/^3\mathrm{He}}(y) g_1^n(x/y,Q^2) + \int_x^3 \frac{dy}{y} \Delta f_{p/^3\mathrm{He}}(y) g_1^p(x/y,Q^2). \tag{1}$$

The motion of the nucleons inside the nucleus (Fermi motion) and their binding are parametrized through the distributions $\Delta f_{N/^3\mathrm{He}}$, which, within the above discussed convention (one variant of the impulse approximation), can be readily calculated using the ground-state wave functions of ^{3}He. Detailed calculations [7–9] by various groups using different ground-state wave functions of ^{3}He came to a similar conclusion that $\Delta f_{N/^3\mathrm{He}}(y)$ are sharply peaked around $y \approx 1$ due to the small average separation energy per nucleon. Thus Eq. (1) is often approximated by

*Email address: fbissey@in2p3.fr
†Email address: vguzey@physics.adelaide.edu.au
‡Email address: strikman@phys.psu.edu
§Email address: athomas@physics.adelaide.edu.au

$$g_1^{^3\mathrm{He}}(x,Q^2)=P_n g_1^n(x,Q^2)+2P_p g_1^p(x,Q^2). \tag{2}$$

Here P_n (P_p) are the effective polarizations of the neutron (proton) inside polarized ^{3}He, which are defined by

$$P_{n,p}=\int_0^3 dy\,\Delta f_{n,p/^3\mathrm{He}}(y). \tag{3}$$

In the first approximation to the ground-state wave function of ^{3}He, only the neutron is polarized, which corresponds to the S-wave type interaction between any pair of the nucleons of ^{3}He. In this case, $P_n=1$ and $P_p=0$. Realistic approaches to the wave function of ^{3}He include also higher partial waves, notably the D and S' partial waves, that arise due to the tensor component of the nucleon-nucleon force. This leads to the depolarization of spin of the neutron and polarization of protons in ^{3}He. The average of calculations with several models of nucleon-nucleon interactions and three-nucleon forces can be summarized as $P_n=0.86\pm0.02$ and $P_p=-0.028\pm0.004$ [10]. The calculations of Ref. [9] give similar values: $P_n=0.879$ and $P_p=-0.021$ for the separable approximation to the Paris potential (PEST) with five channels. We shall use these values for P_n and P_p throughout this paper. One should note that most of the uncertainty in the values for P_n and P_p comes from the uncertainty in the D wave of the ^{3}He wave function. Thus for the observables that are especially sensitive to the poorly constrained P_p, any theoretical predictions bear an uncertainty of at least 10%. An example of such an observable is the point where the neutron structure function g_1^n has a zero.

Equation (1) explicitly assumes that the nuclear spin structure function is given by the convolution with the on-shell nucleon structure functions. In general, the nucleons bound together in a nucleus are subject to off-shell modifications so that the spin structure function of ^{3}He, $g_1^{^3\mathrm{He}}$, should be expressed in terms of the off-shell nucleon spin structure functions $\tilde{g}_1^N$,

$$g_1^{^3\mathrm{He}}(x,Q^2)=\int_x^3\frac{dy}{y}\Delta f_{n/^3\mathrm{He}}(y)\tilde{g}_1^n(x/y,Q^2)+\int_x^3\frac{dy}{y}\Delta f_{p/^3\mathrm{He}}(y)\tilde{g}_1^p(x/y,Q^2). \tag{4}$$

In general, both $\Delta f_{N/^3\mathrm{He}}$ and $\tilde{g}_1^N$ in Eq. (4) depend on the virtuality of the struck nucleon. However, in the region, where the Fermi motion effect is a small correction ($x\leqslant0.7$), one can substitute the off-shell nucleon structure functions by their values at some average virtuality. This was implicitly assumed in Eq. (4).

Off-shell corrections for such a light nucleus as ^{3}He are not expected to be large. In this work, we use the results for $\tilde{g}_1^n$ and $\tilde{g}_1^p$ of Ref. [11], where the off-shell corrections to the valence quark distributions were estimated using the quark meson coupling model [12]. The inclusion of the valence quarks only sets the lower limit of Bjorken x, where the results of Ref. [11] are applicable, e.g., to $x=0.2$. Also, since

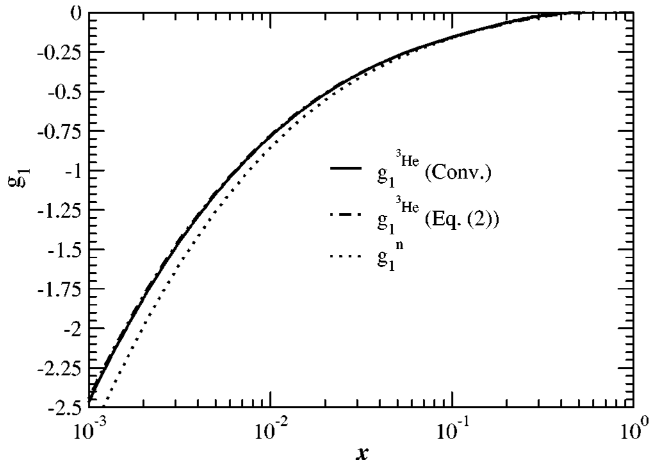

FIG. 1. The spin structure function $g_1^{^3\mathrm{He}}$ obtained with Eq. (4) (solid line) and Eq. (2) (dash-dotted line). The neutron structure function g_1^n is shown as a dotted line.

the quark meson coupling model is based on the MIT bag model, the range of its validity is bound from above by $x\approx0.7$. Thus we apply the results of Ref. [11] at $0.2\leqslant x\leqslant0.7$ and $Q^2\leqslant10$ GeV^2.

The results for the spin structure function $g_1^{^3\mathrm{He}}$ at $Q^2=4$ GeV^2 are presented in Fig. 1. The solid curve depicts $g_1^{^3\mathrm{He}}$ obtained from Eq. (4) with $\Delta f_{N/^3\mathrm{He}}$ obtained using the PEST potential with five channels. This calculation includes all the nuclear effects discussed so far: spin depolarization, Fermi motion and binding, and off-shell effects. We note that on a chosen logarithmic scale along the x axis, the results of Eqs. (4) and (1) are indistinguishable and shown by the solid curve. This should be compared to the dash-dotted curve obtained from Eq. (2), which includes the spin depolarization effects only. Also, for comparison, the neutron spin structure function g_1^n is given by the dotted line. The proton and neutron spin structure functions used in our calculations were obtained using the standard, leading order, polarized parton distributions of Ref. [13].

We would like to stress that the small-x nuclear effects ($10^{-4}\leqslant x\leqslant0.2$), shadowing and antishadowing, were not taken into account so far. While we choose to present our results in Fig. 1 in the region $10^{-3}\leqslant x\leqslant1$ and to discuss our results in the region $10^{-4}\leqslant x\leqslant0.8$ (see below), the most comprehensive expression for the ^{3}He spin structure function, $g_1^{^3\mathrm{He}}$, is discussed in Sec. IV.

As one can see from Fig. 1, the nuclear effects discussed above, among which the most prominent one is nucleon spin depolarization, lead to a sizable difference between $g_1^{^3\mathrm{He}}$ and g_1^n. One finds that $g_1^{^3\mathrm{He}}$ is increased relative to g_1^n by about 10% for $10^{-4}\leqslant x\leqslant0.01$. At larger x, $0.01<x\leqslant0.25$, $g_1^{^3\mathrm{He}}$ and g_1^n are equal with a few percent accuracy. At $x>0.3$ both $g_1^{^3\mathrm{He}}$ and g_1^n are very small so that while a quantitative comparison is possible, it is very sensitive to the details of the calculation. However, one can still make a weakly model-dependent statement that at $x\approx0.45$, where g_1^n is extremely small because it changes sign, the contribution of g_1^p to $g_1^{^3\mathrm{He}}$ becomes at least as important as that of g_1^n.

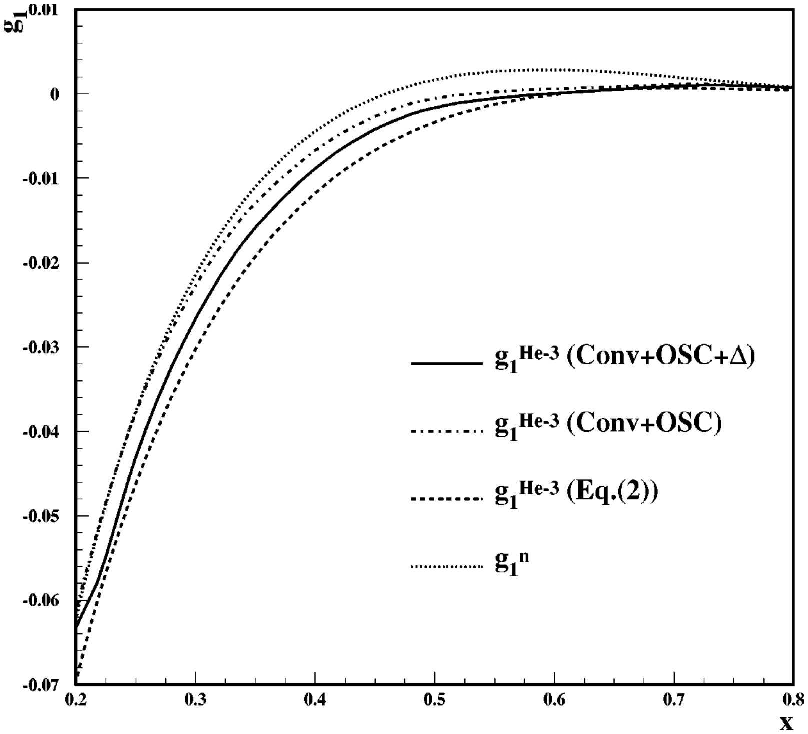

FIG. 2. The spin structure function $g_1^{^3\mathrm{He}}$ obtained from Eq. (17) (solid curve), Eq. (4) (dash-dotted curve), and Eq. (2) (dashed curve). The free neutron spin structure function g_1^n is shown by the dotted curve. For all curves $Q^2=4\ \mathrm{GeV}^2$.

Also, it is important to assess how well Eq. (2) approximates the complete result of Eq. (4). In the region where x is small, $10^{-4}\leqslant x\leqslant 0.1$, Eq. (2) underestimates Eq. (4) by less than 1%. However, for $x>0.2$ the effect of convolution in Eq. (4) makes $g_1^{^3\mathrm{He}}$ sizably larger than predicted by Eq. (2) (see Fig. 2 emphasizing the large-x region). Thus, ignoring for a moment the nuclear shadowing and antishadowing effects, Eq. (2) gives a very good approximation for $g_1^{^3\mathrm{He}}$ over the range $10^{-4}\leqslant x\leqslant 0.1$. At larger x, the complete expression given in Eq. (4) must be used.

Our conclusion that $g_1^{^3\mathrm{He}}$ can be approximated well by Eq. (2) only in the region $10^{-4}\leqslant x\leqslant 0.1$ is more stringent than the earlier result of Ref. [7], where the range of the applicability of Eq. (2) is $10^{-4}\leqslant x\leqslant 0.9$. As an argument in favor of the smaller range of the applicability of Eq. (2), we can consider the so-called European Muon Collaboration (EMC) ratio for the unpolarized DIS on ^{3}He. The deviation of the EMC ratio from unity is, like the deviation of the prediction of Eq. (2) from $g_1^{^3\mathrm{He}}$ based on Eq. (1), a measure of the Fermi motion and binding effects. It was shown in Ref. [14] that the EMC ratio starts to deviate sizably from unity at $x>0.8$. In the work of Ref. [15] this happens already for $x>0.7$.

The convolution approach that forms the basis of Eqs. (1),(2),(4) implies that the nuclear structure function can be obtained through convolution with free and on-shell or off-shell nucleon structure functions. Using a reasonable model for the virtual photon-off-shell nucleon interaction, it was shown in Ref. [16] that the convolution approximation itself breaks down in the region of relativistic kinematics, $x\geqslant 0.8$. Thus $x=0.8$ defines the upper limit for the region of Bjorken x studied in the present work.

It is customary to use Eq. (2) for the extraction of g_1^n from $g_1^{^3\mathrm{He}}$ [3–5]. However, there are other nuclear effects that were not included in Eq. (2) that have also been shown to play an important role in polarized DIS on ^{3}He. These effects include the presence of non-nucleon degrees of freedom and nuclear shadowing and antishadowing.

III. NON-NUCLEONIC DEGREES OF FREEDOM

The description of the nucleus as a mere collection of protons and neutrons is incomplete. In polarized DIS on the trinucleon system, this observation can be illustrated by the following example [17]. The Bjorken sum rule [18] relates the difference of the first moments of the proton and neutron spin structure functions to the axial vector coupling constant of the neutron β decay g_A, where $g_A=1.2670\pm 0.0035$ [19],

$$\int_0^1 [g_1^p(x,Q^2)-g_1^n(x,Q^2)]dx=\frac{1}{6}g_A\left[1+O\left(\frac{\alpha_s}{\pi}\right)\right]. \quad (5)$$

Here the QCD radiative corrections are denoted as "$O(\alpha_s/\pi)$." This sum rule can be straightforwardly generalized to the ^{3}He-^{3}H system:

$$\int_0^3 [g_1^{^3\mathrm{H}}(x,Q^2)-g_1^{^3\mathrm{He}}(x,Q^2)]dx=\frac{1}{6}g_A|_{triton}\left[1+O\left(\frac{\alpha_s}{\pi}\right)\right], \quad (6)$$

where $g_A|_{triton}$ is the axial vector coupling constant of the triton β decay, $g_A|_{triton}=1.211\pm 0.002$ [20]. Taking the ratio of Eqs. (6) and (5), one obtains

$$\frac{\int_0^3 [g_1^{^3\mathrm{H}}(x,Q^2)-g_1^{^3\mathrm{He}}(x,Q^2)]dx}{\int_0^1 [g_1^p(x,Q^2)-g_1^n(x,Q^2)]dx}=\frac{g_A|_{triton}}{g_A}=0.956\pm 0.004. \tag{7}$$

Note that the QCD radiative corrections are expected to cancel exactly[1] in Eq. (7).

Assuming charge symmetry between the ^{3}He and ^{3}H ground-state wave functions, one can write the triton (^{3}H) spin structure function $g_1(x,Q^2)$ in the form [see Eq. (4)]

$$g_1^{^3\mathrm{H}}(x,Q^2)=\int_x^3 \frac{dy}{y}\Delta f_{n/^3\mathrm{He}}(y)\tilde{g}_1^p(x/y,Q^2) + \int_x^3 \frac{dy}{y}\Delta f_{p/^3\mathrm{He}}(y)\tilde{g}_1^n(x/y,Q^2). \tag{8}$$

Combining Eqs. (4) and (8) and using the fact that, for example,

$$\int_0^3 dx \int_x^3 \frac{dy}{y}\Delta f_{n/^3\mathrm{He}}(y)\tilde{g}_1^n(x/y,Q^2) = \int_0^3 dy \Delta f_{n/^3\mathrm{He}}(y)\int_0^1 dx \tilde{g}_1^n(x,Q^2)=P_n\int_0^1 dx\tilde{g}_1^n(x,Q^2), \tag{9}$$

one obtains the following estimate for the ratio of the nuclear to nucleon Bjorken sum rules

$$\frac{\int_0^3 [g_1^{^3\mathrm{H}}(x,Q^2)-g_1^{^3\mathrm{He}}(x,Q^2)]dx}{\int_0^1 [g_1^p(x,Q^2)-g_1^n(x,Q^2)]dx} = (P_n-2P_p)\frac{\tilde{\Gamma}_p-\tilde{\Gamma}_n}{\Gamma_p-\Gamma_n}=0.921\frac{\tilde{\Gamma}_p-\tilde{\Gamma}_n}{\Gamma_p-\Gamma_n}. \tag{10}$$

Here we used $P_n=0.879$ and $P_p=-0.021$; $\tilde{\Gamma}_N=\int_0^1 dx\tilde{g}_1^N(x)$ and $\Gamma_N=\int_0^1 dx g_1^N(x)$.

If anything, the off-shell corrections of Ref. [11] decrease rather than increase the bound nucleon spin structure functions [i.e., $(\tilde{\Gamma}_p-\tilde{\Gamma}_n)/(\Gamma_p-\Gamma_n)<1$]. Thus one can immediately see that the theoretical prediction for the ratio of the Bjorken sum rule for the $A=3$ and $A=1$ systems [Eq. (10)], based solely on nucleonic degrees of freedom, underestimates the experimental result for the same ratio [Eq. (7)] by about 3.5%. This demonstrates the need for new nuclear effects that are not included in Eqs. (1),(2),(4).

It has been known for a long time that non-nucleonic degrees of freedom, such as pions, vector mesons, the $\Delta(1232)$ isobar, play an important role in the calculation of low-energy observables of nuclear physics. In particular, the analyses of Ref. [21] demonstrated that the two-body exchange currents involving a $\Delta(1232)$ isobar increase the theoretical prediction for the axial vector coupling constant of triton by about 4%, which makes it consistent with experiment. Consequently, exactly the same mechanism must be present in case of deep inelastic scattering on polarized ^{3}He and ^{3}H. Indeed, as explained in Refs. [17,22], the direct correspondence between the calculations of the Gamow-Teller matrix element in the triton β decay and the Feynman diagrams of DIS on ^{3}He and ^{3}H (see Fig. 1 of [22]) requires that two-body exchange currents should play an equal role in both processes. As a result, the presence of the Δ in the ^{3}He and ^{3}H wave functions should increase the ratio of Eq. (10) and make it consistent with Eq. (7).

The contribution of the $\Delta(1232)$ to $g_1^{^3\mathrm{He}}$ is realized through Feynman diagrams involving the nondiagonal interference transitions $n\to\Delta^0$ and $p\to\Delta^+$. This requires new spin structure functions $g_1^{n\to\Delta^0}$ and $g_1^{p\to\Delta^+}$, as well as the effective polarizations $P_{n\to\Delta^0}$ and $P_{p\to\Delta^+}$. Taking into account the interference transitions, the spin structure functions $g_1^{^3\mathrm{He}}$ and $g_1^{^3\mathrm{H}}$ can be written as

$$\begin{aligned} g_1^{^3\mathrm{He}}&=\int_x^3 \frac{dy}{y}\Delta f_{n/^3\mathrm{He}}(y)\tilde{g}_1^n(x/y,Q^2)+\int_x^3\frac{dy}{y}\Delta f_{p/^3\mathrm{He}}(y)\\ &\quad\times\tilde{g}_1^p(x/y,Q^2)+2P_{n\to\Delta^0}g_1^{n\to\Delta^0}+4P_{p\to\Delta^+}g_1^{p\to\Delta^+},\\ g_1^{^3\mathrm{H}}&=\int_x^3 \frac{dy}{y}\Delta f_{n/^3\mathrm{He}}(y)\tilde{g}_1^p(x/y,Q^2)+\int_x^3\frac{dy}{y}\Delta f_{p/^3\mathrm{He}}(y)\\ &\quad\times\tilde{g}_1^n(x/y,Q^2)-2P_{n\to\Delta^0}g_1^{p\to\Delta^+}-4P_{p\to\Delta^+}g_1^{n\to\Delta^0}. \end{aligned} \tag{11}$$

The minus sign in front of the interference terms in the expression for $g_1^{^3\mathrm{H}}$ originates from the sign convention $P_{n\to\Delta^0}\equiv P_{n\to\Delta^0/^3\mathrm{He}}=-P_{p\to\Delta^+/^3\mathrm{H}}$ and $P_{p\to\Delta^+}\equiv P_{p\to\Delta^+/^3\mathrm{He}}=-P_{n\to\Delta^0/^3\mathrm{H}}$. Note that in general the interference spin structure functions should be convoluted with the corresponding light-cone momentum distributions. However, modeling such distributions is beyond the scope of the present work. Instead, for simplicity, the convolution is approximated by the effective polarizations $P_{n\to\Delta^0}$ and $P_{p\to\Delta^+}$, just like Eq. (2) approximates Eq. (1).

The interference structure functions $g_1^{n\to\Delta^0}$ and $g_1^{p\to\Delta^+}$, as well structure functions for the octet of baryons and the decuplet of baryon resonances, can be estimated using the following considerations. Starting from the most general expression for the quark distribution in a baryon, and using the MIT bag model with a spin-dependent hyperfine interaction between the quarks, one can express the proton, neutron, and interference structure functions as [23]

[1] Within the formalism of the operator product expansion, the Q^2 dependence of moments of DIS structure functions is given by target-independent coefficient functions. Hence QCD radiative corrections in Eq. (6) are the same as in Eq. (5).

$$g_1^p(x,Q_0^2)=\frac{1}{18}[6G_s(x,Q_0^2)-G_v(x,Q_0^2)],$$

$$g_1^n(x,Q_0^2)=\frac{1}{12}[G_s(x,Q_0^2)-G_v(x,Q_0^2)],$$

$$g_1^{n\to\Delta^0}=g_1^{p\to\Delta^+}=\frac{\sqrt{2}}{9}G_v(x,Q_0^2). \qquad (12)$$

Here G_s and G_v are the contributions associated with scalar and vector spectator diquarks inside the bag. Note that SU(6) symmetry of the baryon wave function is implicitly broken by the hyperfine interaction in Eq. (12), which means that $G_s \neq G_v$.

Instead of using the MIT bag model to evaluate G_s and G_v, and hence $g_1^{n\to\Delta^0}$ and $g_1^{p\to\Delta^+}$, we choose to relate the latter to g_1^p and g_1^n. Using Eq. (12), one observes that

$$g_1^{n\to\Delta^0}=g_1^{p\to\Delta^+}=\frac{2\sqrt{2}}{5}(g_1^p-4g_1^n). \qquad (13)$$

We would like to emphasize that the derivation of Eq. (13) does not require SU(6) symmetry, which is known to fail badly for the nucleon spin structure functions. Also, since the derivation assumes that baryons and their resonances consist of three constituent quarks, we expect relationship (13) to hold in the region of x and Q^2, where the distribution of polarized valence quarks dominates polarized sea quarks and gluons. Using the parametrization of Ref. [13], we estimate this region[2] to be $0.5 \leqslant Q^2 \leqslant 5$ GeV^2 and $0.2 \leqslant x \leqslant 0.8$.

In principle, the effective polarizations of the interference contributions $P_{n\to\Delta^0}$ and $P_{p\to\Delta^+}$ can be calculated using a ^{3}He wave function that includes the Δ resonance. This is an involved computational problem. Instead, we chose to find $P_{n\to\Delta^0}$ and $P_{p\to\Delta^+}$ by *requiring* that the use of the ^{3}He and ^{3}H structure functions of Eq. (11) gives the experimental ratio of the nuclear to nucleon Bjorken sum rules (7). Substituting Eq. (11) into Eq. (7) yields

$$-2(P_{n\to\Delta^0}+2P_{p\to\Delta^+})\frac{\int_0^1 dx[g_1^{n\to\Delta^0}(x)+g_1^{p\to\Delta^+}(x)]}{\Gamma_p-\Gamma_n}$$
$$=0.956-0.921\frac{\tilde{\Gamma}_p-\tilde{\Gamma}_n}{\Gamma_p-\Gamma_n}. \qquad (14)$$

Next, we use Eq. (13) to relate the interference structure functions to the off-shell modified proton and neutron spin structure functions and to obtain

$$2(P_{n\to\Delta^0}+2P_{p\to\Delta^+})=\frac{0.814(\tilde{\Gamma}_p-\tilde{\Gamma}_n)-0.845(\Gamma_p-\Gamma_n)}{\tilde{\Gamma}_{p'}-4\tilde{\Gamma}_{n'}}. \qquad (15)$$

Here $\tilde{\Gamma}_{p'}$ ($\tilde{\Gamma}_{n'}$) is the proton (neutron) off-shell modified spin structure function integrated over the interval $0.2 \leqslant x \leqslant 0.8$. Using the standard parametrization of Ref. [13] and the results for the off-shell corrections of Ref. [11], we find for the necessary combination of the effective polarizations:

$$2(P_{n\to\Delta^0}+2P_{p\to\Delta^+})=-0.024. \qquad (16)$$

Note that Eq. (16) gives a value that is very similar to the one reported in our original publication [22].

Equations (11,13,16) enable one to write an explicit expression for the ^{3}He spin structure function, which takes into account the additional Feynman diagrams corresponding to the nondiagonal interference $n\to\Delta^0$ and $p\to\Delta^+$ transitions (see Fig. 1 of [22]) and which complies with the experimental value of the ratio of the Bjorken sum rules (7):

$$g_1^{^3\mathrm{He}}=\int_x^3\frac{dy}{y}\Delta f_{n/^3\mathrm{He}}(y)\tilde{g}_1^n(x/y,Q^2)+\int_x^3\frac{dy}{y}\Delta f_{p/^3\mathrm{He}}(y)$$
$$\times\tilde{g}_1^p(x/y,Q^2)-0.014[\tilde{g}_1^p(x,Q^2)-4\tilde{g}_1^n(x,Q^2)]. \qquad (17)$$

Note that the last term in Eq. (17) should be included only in the region $0.2 \leqslant x \leqslant 0.8$.

The results of the calculation of $g_1^{^3\mathrm{He}}$ at $Q^2=4$ GeV^2 based on Eq. (17) are presented in Fig. 2 as a solid curve. They should be compared to $g_1^{^3\mathrm{He}}$ obtained from Eq. (4) (dash-dotted curve) and to $g_1^{^3\mathrm{He}}$ obtained from Eq. (2) (dashed line). The neutron spin structure function g_1^n is given by the dotted curve.

One can see from Fig. 2 that the presence of the $\Delta(1232)$ isobar in the ^{3}He wave function works to decrease $g_1^{^3\mathrm{He}}$ relative to the prediction of Eq. (4). This decrease is 12% at $x=0.2$ and increases at larger x, peaking for $x\approx 0.46$, where g_1^n changes sign.

Equation (17) describes the nuclear effects of the nucleon spin depolarization and the presence of non-nucleon degrees of freedom in the ^{3}He ground-state wave function and is based on the convolution formula (1). Since the convolution formalism implies *incoherent* scattering off nucleons and nucleon resonances of the target, coherent nuclear effects present at small values of Bjorken x are ignored. In the next section we demonstrate the role played by two coherent effects, nuclear shadowing and antishadowing, in DIS on polarized ^{3}He.

IV. NUCLEAR SHADOWING AND ANTISHADOWING

At high energies or small Bjorken x, the virtual photon can interact coherently with several nucleons in the nuclear target. This is manifested in a specific behavior of nuclear structure functions that cannot be accommodated by the con-

[2]The lower limit of applicability of Eq. (13), $x=0.2$, is chosen such that for $x \geqslant 0.2$ the contribution of the polarized sea quarks and gluons to g_1^p and g_1^n is five times smaller than that of the polarized valence quarks.

volution approximation. In particular, by studying DIS of muons on a range of unpolarized nuclear targets, the NMC collaboration [24] demonstrated that the ratio $2F_2^A/(AF_2^D)$ deviates significantly from unity: it is smaller than unity for $0.0035 \leqslant x \leqslant 0.03$–$0.07$ and is larger than unity for 0.03–$0.07 \leqslant x \leqslant 0.2$. The depletion of the ratio $2F_2^A/(AF_2^D)$ is called nuclear shadowing, while the enhancement is termed nuclear antishadowing. Both of the effects break down the convolution approximation.

Quite often nuclear targets are used in polarized DIS experiments. While these experiments do not reach such low values of x as the unpolarized fixed target experiments, where nuclear shadowing is important, the antishadowing region is still covered. In the absence of a firm theoretical foundation, nuclear shadowing and antishadowing have been completely ignored in the analysis of the DIS data on polarized nuclei. The prime motivation of this section is to demonstrate that these two effects are quite significant and do affect the extraction of the nucleon spin functions from the nuclear data.

The physical picture of nuclear shadowing in DIS is especially transparent in the target rest frame. At high energy, the incident photon, $|\gamma^*\rangle$, interacts with hadronic targets by fluctuating into hadronic configurations $|h_k\rangle$, long before it hits the target:

$$|\gamma^*\rangle = \sum_k \langle h_k|\gamma^*\rangle |h_k\rangle, \tag{18}$$

where "k" is a generic label for the momentum and helicity of the hadronic fluctuation h_k. Thus the total cross section for virtual photon-nucleus scattering, $\sigma^{tot}_{\gamma^* A}$, can be presented in the general form

$$\sigma^{tot}_{\gamma^* A} = \sum_k |\langle h_k|\gamma^*\rangle|^2 \sigma^{tot}_{h_k A}. \tag{19}$$

Here $|\langle h_k|\gamma^*\rangle|^2$ is the probability of the fluctuation $|\gamma\rangle \to |h_k\rangle$; $\sigma^{tot}_{h_k A}$ is the $|h_k\rangle$-nucleus total cross section. In obtaining Eq. (19) from Eq. (18) we assumed that the fluctuations h_k do not mix during the interaction. In general, this is not true since various configurations $|h_k\rangle$ contribute to expansion (18), and those states are not eigenstates of the scattering matrix, i.e., they mix. However, one can replace the series (18) by an effective state $|h_{\rm eff}\rangle$ (for details of the calculation see Appendix) so that Eq. (19) simplifies

$$\sigma^{tot}_{\gamma^* A} = |\langle h_{\rm eff}|\gamma^*\rangle|^2 \sigma^{tot}_{h_{\rm eff} A}. \tag{20}$$

Since the effective hadronic fluctuation $h_{\rm eff}$ can interact coherently with several nucleons of the target, the total scattering cross section on the nucleus is smaller than the sum of the cross sections on individual nucleons, i.e., nuclear shadowing takes place and $\sigma^{tot}_{h_{\rm eff}A} < A\sigma^{tot}_{h_{\rm eff}N}$. This leads to $\sigma^{tot}_{\gamma^* A} < A\sigma^{tot}_{\gamma^* N}$ and to shadowing of the nuclear structure functions. The approximation by a single effective state [see Eq. (20)] was used to estimate the nuclear shadowing correction to spin structure functions of deuterium [25], ^{3}He [17,26], ^{7}Li [26], and ^{6}LiD [27].

By definition, the spin structure function $g_1^{^3\rm He}$ can be expressed as

$$g_1^{^3\rm He} \propto \sigma^{\uparrow\uparrow}_{\gamma^* {}^3\rm He} - \sigma^{\uparrow\downarrow}_{\gamma^* {}^3\rm He} \propto \sigma^{\uparrow\uparrow}_{h_{\rm eff}{}^3\rm He} - \sigma^{\uparrow\downarrow}_{h_{\rm eff}{}^3\rm He}, \tag{21}$$

where $\sigma^{\uparrow\uparrow}_{h_{\rm eff}{}^3\rm He}$ ($\sigma^{\uparrow\downarrow}_{h_{\rm eff}{}^3\rm He}$) is the cross section for the scattering when the helicities of the projectile and the nucleus are parallel (antiparallel). The cross sections $\sigma^{\uparrow\uparrow}_{h_{\rm eff}{}^3\rm He}$ and $\sigma^{\uparrow\downarrow}_{h_{\rm eff}{}^3\rm He}$ can be calculated using the standard Gribov-Glauber multiple scattering formalism. Within this approach, $\sigma^{\uparrow\uparrow}_{h_{\rm eff}{}^3\rm He}$ and $\sigma^{\uparrow\downarrow}_{h_{\rm eff}{}^3\rm He}$ receive contributions from the virtual photon scattering on each nucleon, each pair of nucleons, and all three nucleons of the target. The first kind of contribution corresponds to incoherent scattering on the nucleons and leads to $g_1^{^3\rm He}$ as given by Eq. (4). The simultaneous, coherent scattering on pairs of nucleons and all three of them results in the shadowing correction to $g_1^{^3\rm He}$, $\delta g_1^{^3\rm He}$. Detailed calculations of $\delta g_1^{^3\rm He}$ are presented in the Appendix. Thus, including the nuclear shadowing correction, the spin structure function of ^{3}He reads

$$g_1^{^3\rm He} = \int_x^3 \frac{dy}{y}\Delta f_{n/^3\rm He}(y)\tilde{g}_1^n(x/y) + \int_x^3 \frac{dy}{y}\Delta f_{p/^3\rm He}(y)\tilde{g}_1^p(x/y) - 0.014[\tilde{g}_1^p(x) - 4\tilde{g}_1^n(x)] + a^{sh}(x)g_1^n(x) + b^{sh}(x)g_1^p(x), \tag{22}$$

where a^{sh} and b^{sh} are functions of x and Q^2 and are calculated using a particular model for nuclear shadowing and a specific form of the ^{3}He ground-state wave function.

The present accuracy of fixed target polarized DIS experiments on nuclear targets is not sufficient for dedicated studies of nuclear shadowing. Thus one can only use information obtained from unpolarized DIS on nuclei. All of those experiments—NMC at CERN, a number of experiments at SLAC, BCDMS, and E665 at Fermilab—demonstrated that nuclear shadowing at $10^{-4} \leqslant x \leqslant 0.03$–$0.07$ is followed by some antishadowing at 0.03–$0.07 \leqslant x \leqslant 0.2$. It is natural to assume a similar pattern for polarized DIS on ^{3}He. Thus Eq. (22) can be generalized as

$$g_1^{^3\rm He} = \int_x^3 \frac{dy}{y}\Delta f_{n/^3\rm He}(y)\tilde{g}_1^n(x/y) + \int_x^3 \frac{dy}{y}\Delta f_{p/^3\rm He}(y)\tilde{g}_1^p(x/y) - 0.014[\tilde{g}_1^p(x) - 4\tilde{g}_1^n(x)] + a(x)g_1^n(x) + b(x)g_1^p(x), \tag{23}$$

where a (b) coincide with a^{sh} (b^{sh}) in the nuclear shadowing region of Bjorken x and model antishadowing at larger x. Since the shadowing contribution in Eq. (22) breaks the equivalence of the theoretical and experimental values for the ratio of the nuclear to nucleon Bjorken sum rules, one can reinstate the equivalence by a suitable choice of antishadowing. Thus we model antishadowing by requiring that Eq. (23) and its ^{3}H counterpart give the correct ratio in Eq. (7). Substituting Eq. (23) into Eq. (7), we obtain the following condition on the functions a and b:

$$\int_{10^{-4}}^{0.2} dx[a(x)-b(x)][g_1^p(x)-g_1^n(x)]=0. \tag{24}$$

Note that the the lower limit of integration, $x=10^{-4}$, is somewhat artificial since it is defined by the range of x covered by the parametrizations of g_1^p and g_1^n of Ref. [13]. The upper limit of integration, $x=0.2$, is defined by the following consideration. We expect that antishadowing is related to coherent interactions with several nucleons of the target, similarly to nuclear shadowing. Since the coherence length, $l_{\rm coh} \approx 1/(2m_N x)$, becomes smaller than the average internucleon distance, $r_{NN}\approx 2$ fm, for $x>0.2$, we do not expect any coherent effects, including antishadowing, for those values of x. It is natural to assume that one coherent effect (shadowing) is compensated by another coherent effect (antishadowing) in the Bjorken sum rule and in Eq. (24).

In general, the functions a and b are independent. In order to simplify the modeling of a and b in the antishadowing region, we assume that they are proportional to each other, i.e., $a(x)=cb(x)$, where c is a constant. Our calculations of a and b in the nuclear shadowing region (where $a=a^{sh}$ and $b=b^{sh}$) justify this assumption with high accuracy and enable us to fix the value for the constant c: $c=57$. The value of the coefficient c reflects the dominance of the effective polarization of the neutron, P_n, over that of the proton, P_p. Equation (24) determines the net contribution of $a(x)$ and $b(x)$ to the Bjorken sum rule, but does not fix the shapes of $a(x)$ and $b(x)$. In our analysis we assumed a quadratic polynomial form for $a(x)$ and $b(x)$ such that both functions exist on the interval $x_0\leqslant x\leqslant 0.2$ and vanish at the end points.

Nuclear shadowing is followed by some antishadowing. The crossover point between the two regions, x_0, is a parameter, which should be inferred from experiment. Unfortunately, even the most precise NMC data [24] is inconclusive about the exact position of the crossover point x_0: experimental errors allow x_0 to be positioned anywhere between 0.03 and 0.07. In order to take into account this ambiguity, which constitutes major theoretical uncertainty of our treatment of antishadowing, we considered two extreme versions: $x_0=0.03$ and $x_0=0.07$.

As explained in detail in the Appendix, in calculating the shadowing correction $\delta g_1^{^3\mathrm{He}}$ and a^{sh} and b^{sh} entering Eq. (22) we used two versions of the model by Frankfurt and Strikman [28]. In this model, the nuclear shadowing correction to the nuclear structure function F_2^A is inferred using a connection to the proton diffractive structure function F_2^D. Both structure functions, F_2^A and F_2^D, enter unpolarized DIS. However, we still choose to use this model to evaluate nuclear shadowing in polarized DIS. In principle, if the data on polarized electron-proton diffraction existed, one could readily improve our treatment of nuclear shadowing in polarized DIS on nuclei, using the formalism developed in Ref. [28]. One of the main reasons why we decided to use the results of Ref. [28] is because this model corresponds to the leading twist shadowing correction to the nuclear parton densities, i.e., nuclear shadowing decreases logarithmically with Q^2 according to the QCD evolution equation. We are forced to use the leading twist model of nuclear shadowing because in order to model the antishadowing contribution, we will use the Bjorken sum rule, which is a leading twist result.

Alternatively, if we were not concerned with leading twist shadowing, we could use another model for nuclear shadowing. For example, the data on inclusive nuclear structure functions were successfully described within the two-phase model of Refs. [29]. This model contains both the leading twist (Pomeron and triple Pomeron exchanges) and subleading twist (vector meson) contributions. The latter contribution is required to describe the data at low x and low Q^2, where higher twist effects are expected to be important. Thus, in applying shadowing corrections to low-Q^2 data points (such as the HERMES data used in our analysis), one should be aware of the higher twist effects, which will make predictions less model independent.

Results for the function a calculated with $x_0=0.03$ and $x_0=0.07$ are presented in Fig. 3 at $Q^2=4$ GeV^2. In both cases the amount of nuclear shadowing at small x is quite similar: at $x=10^{-4}$, the shadowing correction amounts to 11%, when $x_0=0.03$, and to 12%, when $x_0=0.07$. These results are consistent with the earlier results of Refs. [17,26], where the shadowing correction to $g_1^{^3\mathrm{He}}$ was of the order 10%. Moreover, such a good consistency between the present calculation using the exact wave function of ^{3}He and the calculations using a simple Gaussian shape for the ^{3}He wave function, where only the neutron was polarized [17,26], demonstrates that higher partial waves (S' and D) are unimportant in the calculation of the shadowing correction for polarized ^{3}He.

By choosing two different crossover points, we can assess the theoretical uncertainty of our modeling of antishadowing. Since a^{sh} in the model with the crossover point $x_0=0.07$ occupies a narrower region of x, the corresponding a in the antishadowing region reaches higher values relative to the model with $x_0=0.03$. For instance, at its maximum the antishadowing correction is of the order 3%, when $x_0=0.03$, and of the order 7%, when $x_0=0.07$. These values for the antishadowing correction are significantly smaller than those reported in Refs. [17,26]. This discrepancy must have arisen from slightly different shapes of the x dependence of antishadowing and different parametrizations for g_1^p and g_1^n, which enter Eq. (24) and determine the magnitude of antishadowing.

Our assumption that nuclear shadowing and antishadowing compensate each other in the Bjorken sum rule is quite strong. However, we do not know how to improve on our approximation at the moment since a qualitatively different approach is required. In general, all three effects—nuclear shadowing, antishadowing, and the Δ isobar—contribute simultaneously to the Bjorken sum rule and the relative importance of these effects to the integral could be different from that assumed in this work. For instance, one could neglect

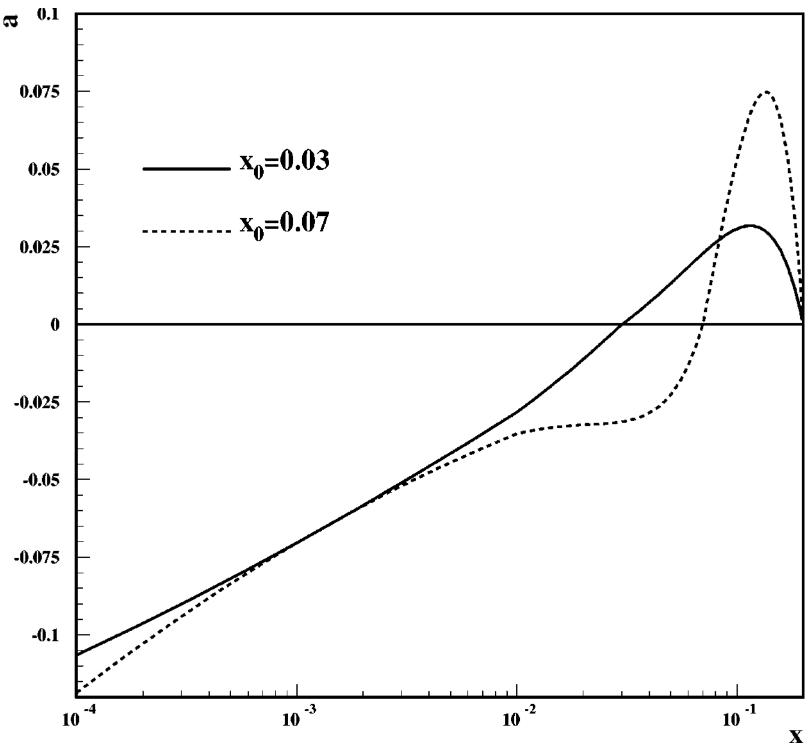

FIG. 3. The coefficient a entering Eq. (23) that describes nuclear shadowing and antishadowing corrections. The solid curve corresponds to $x_0=0.03$; the dashed curve corresponds to $x_0=0.07$.

antishadowing altogether and still have the theoretical prediction for the ratio of the Bjorken sum rules in agreement with the value extracted from experiment by a suitable choice of the effective polarizations $P_{n\to\Delta^0}$ and $P_{p\to\Delta^+}$. However, our experience from unpolarized DIS on nuclei suggests that such a scenario is unlikely.

One should note that our approach to antishadowing based on the ratio of the Bjorken sum rules [see Eq. (7)] is the only example of modeling of antishadowing for polarized DIS on nuclei known in the literature. An improvement on this approximation would require a major theoretical development in understanding the mechanism of nuclear shadowing and antishadowing for parton distributions driven by exchanges with nonvacuum quantum numbers, i.e., by non-Pomeron exchanges. To approach the solution, one should possibly start from unpolarized DIS, where baryon and momentum sum rules give powerful constraints on the shape of parton distributions in nuclei. In unpolarized DIS on nuclei, models of antishadowing include the model of Ref. [30], where antishadowing explained by introducing both the Pomeron and Reggeon exchanges (there is only the Pomeron exchange in the present work) for the virtual photon-nucleon interaction, and the model of Ref. [31], where antishadowing is a consequence of the virtual photon scattering off the pion cloud of the nucleus and nucleon-nucleon correlations in the nuclear wave function. Unfortunately, it is not clear if the baryon number and momentum sum rules are conserved in these two models.

Using our calculations for the coefficients a and b, we present the most comprehensive result for the ^{3}He spin structure function $g_1^{^3\mathrm{He}}$ based on Eq. (23) in Fig. 4. The solid curve includes all of the effects discussed above: nucleon spin depolarization, Fermi motion and binding effects, the presence of the Δ isobar in the ^{3}He wave function, and nuclear shadowing and antishadowing. On the chosen scale, the results of the calculations with the two different crossover points x_0 are indistinguishable and are shown by the same solid curve. This should be compared to the calculation of $g_1^{^3\mathrm{He}}$ based on Eq. (2) (dashed curve) and to the free neutron spin structure function g_1^n (dotted curve).

The comparison between the solid and the dashed curves is very important and constitutes one of the main results of the present work. So far, in the analysis of all experiments on DIS on polarized ^{3}He—the E142 and E154 experiments at SLAC and the HERMES experiment at DESY—it was assumed that the ^{3}He spin structure function $g_1^{^3\mathrm{He}}$ can be represented well by Eq. (2). However, the sizable difference between the full calculation based on Eq. (23) and the one based on Eq. (2) indicates that it is important to treat all the relevant nuclear effects equally carefully. In the nuclear shadowing region, $10^{-4}\leqslant x\leqslant 0.03$–$0.07$, $g_1^{^3\mathrm{He}}$ based on Eq. (23) is larger than that based on Eq. (2). For example, at $x=10^{-3}$ the difference is 8%. In the antishadowing region, 0.03–$0.07<x\leqslant 0.2$, $g_1^{^3\mathrm{He}}$ based on Eq. (23) is smaller than the one predicted by Eq. (2). The difference can be read off from the corresponding curves for the function a from Fig. 3. For instance, for the calculation with $x_0=0.07$, the full result for $g_1^{^3\mathrm{He}}$ is smaller than the approximate one of Eq. (2) by 7% at $x=0.13$. Since nuclear shadowing and antishadowing are absent at $x>0.2$, Eq. (23) coincides with Eq. (7) in this region and for the comparison between the full calculations and an approximate one given by Eq. (2), we refer the reader to the discussion of Fig. 2.

V. EXTRACTION OF g_1^n FROM THE ^{3}He DATA

In the previous section we presented the calculation of the spin structure function of ^{3}He, $g_1^{^3\mathrm{He}}$, which includes the

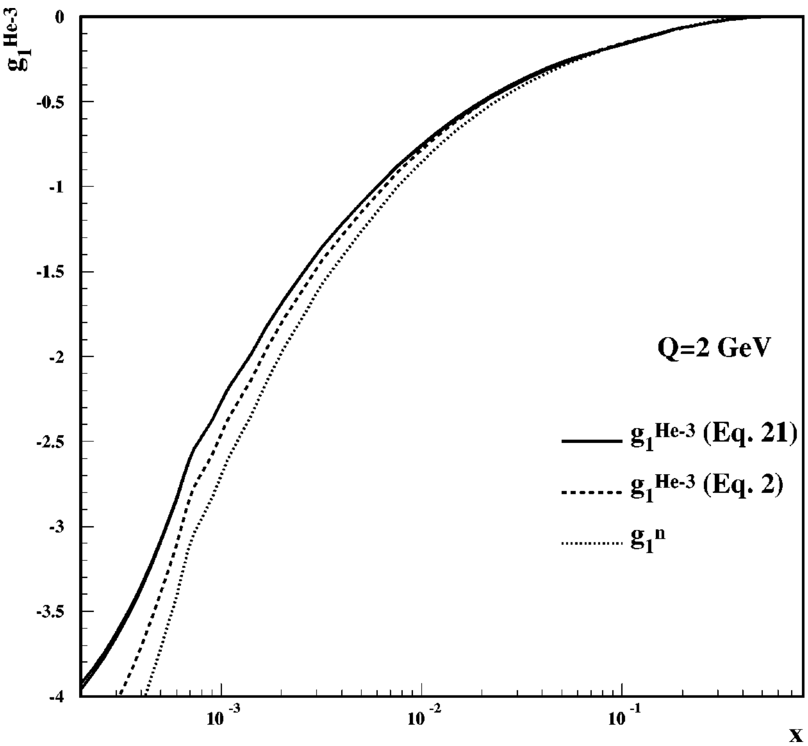

FIG. 4. The full calculation of $g_1^{^3\mathrm{He}}$ including nuclear shadowing and antishadowing based on Eq. (23) (two solid curves) compared to the result of Eq. (2) (dashed curve) and to g_1^n (dotted curve).

effects of nuclear shadowing and antishadowing, the presence of the $\Delta(1232)$ isobar in the ^{3}He wave function, nucleon spin depolarization, Fermi motion and binding, and off-shellness of the nucleons. The resulting $g_1^{^3\mathrm{He}}$ given by Eq. (23) deviates from the approximate expression for $g_1^{^3\mathrm{He}}$ given by Eq. (2), which takes into account only the effect of the nucleon spin depolarization. Since Eq. (2) was used to extract the neutron spin structure function g_1^n from $g_1^{^3\mathrm{He}}$, one should reanalyse the data using the complete Eq. (23). In particular, we present our corrections to g_1^n obtained from DIS on polarized ^{3}He by the E154 Collaboration at SLAC [5] and the HERMES Collaboration at DESY [4].

Let us denote the neutron structure function obtained from $g_1^{^3\mathrm{He}}$, using Eq. (2), as $g_{1\,\mathrm{exp}}^n$. On the other hand, the "true" neutron structure function, g_1^n, should be extracted from Eq. (23). First, our analysis (see Fig. 1 and the discussion of it) demonstrates that the off-shell corrections are negligible. Second, as can be seen by comparing the dash-dotted and dotted curves in Fig. 2, Fermi motion and binding do matter for $x>0.1$. Thus in order to extract g_1^n from Eq. (23) one must deconvolute this expression, which would involve a number of approximations and would bear a significant theoretical uncertainty. We opt for a simpler option—which possibly has similar degree of accuracy—of replacing the convolution in Eq. (23) by the effective polarizations:

$$g_1^{^3\mathrm{He}}=P_n g_1^n+2P_p g_1^p-0.014[g_1^p(x)-4g_1^n(x)] \\ +a(x)g_1^n(x)+b(x)g_1^p(x). \tag{25}$$

Besides its simplicity, Eq. (25) also clearly indicates which nuclear effects contribute to $g_1^{^3\mathrm{He}}$. Thus the influence of the effects of nuclear shadowing and antishadowing and the Δ isobar on the g_1^n extracted from the ^{3}He data can be represented by the ratio of g_1^n based on Eq. (25) to $g_{1\,\mathrm{exp}}^n$

$$\frac{g_1^n}{g_{1\,\mathrm{exp}}^n}=\frac{P_n+g_1^p/g_{1\,\mathrm{exp}}^n[0.014-b(x)]}{P_n+0.056+a(x)}. \tag{26}$$

Note that the coefficients 0.014 and 0.056 should be set to zero for $x<0.2$ and $x>0.8$. By definition, the functions a and b are equal to zero for $x\geqslant 0.2$.

The results of the application of Eq. (26) to $g_{1\,\mathrm{exp}}^n$ reported by the E154 and HERMES Collaborations are presented in Fig. 5. We present calculations for the case, when $x_0=0.07$. For simplicity we assumed that the functions a and b entering Eq. (26) and describing the amount of nuclear shadowing and antishadowing do not vary appreciably with Q^2. This enabled us to use our results for a and b at fixed $Q^2=4\ \mathrm{GeV}^2$, which were presented in the previous section (see Fig. 3). The proton spin structure function g_1^p was evaluated at the appropriate x and Q^2 using the parametrization of Ref. [13]. Also note that while the values of x and Q^2 are correlated for the HERMES data, the E154 Collaboration has evolved their data to the common scale $Q^2=5\ \mathrm{GeV}^2$.

One can see from Fig. 5 that in the region of nuclear shadowing, $10^{-4}\leqslant x\leqslant 0.07$, ignoring nuclear shadowing would lead one to overestimate g_1^n. For the lowest-x experimental data points, this effect is of the order 4%. At larger x, $0.07\leqslant x\leqslant 0.2$, the inclusion of nuclear antishadowing increases g_1^n. For instance, the increase is 7% at $x\approx 0.12$–0.13, where the antishadowing correction is maximal. The influence of the Δ isobar on the extraction of g_1^n

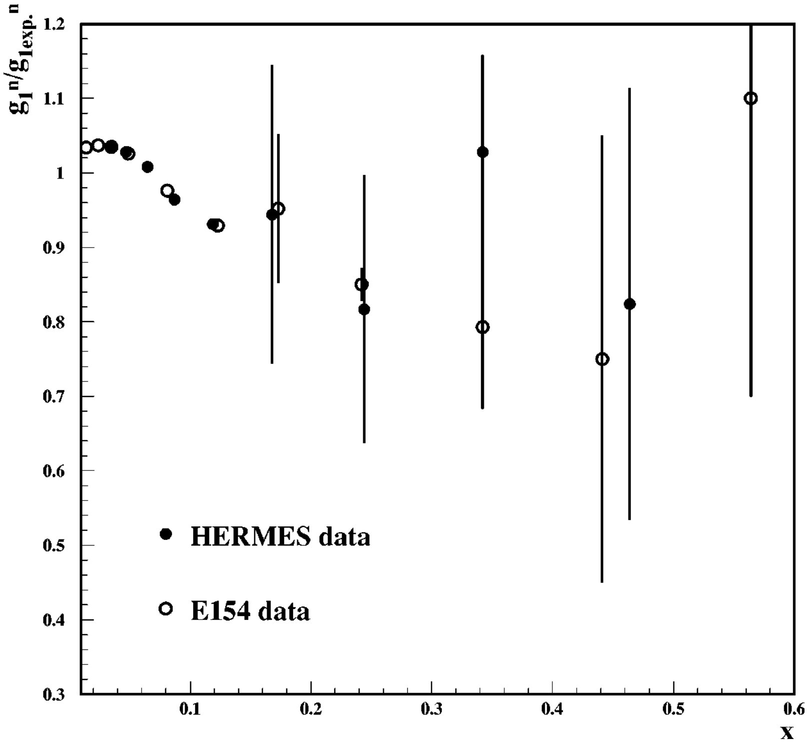

FIG. 5. The ratio $g_1^n/g_{1\ \mathrm{exp}}^n$ based on Eq. (26), which demonstrates how the HERMES [4] and E154 [5] values for $g_{1\ \mathrm{exp}}^n$ should be corrected to include nuclear shadowing, antishadowing, and the Δ isobar effects. The statistical uncertainty of $g_{1\ \mathrm{exp}}^n$ contributes to the uncertainty of our predictions for $g_1^n/g_{1\ \mathrm{exp}}^n$, which is shown by vertical lines.

from the ^{3}He data is even larger: the experimental values for g_1^n should be increased by as much as 15–25 %.

It is also interesting to note that the correction associated with the presence of the Δ isobar changes the value of Bjorken x, where g_1^n changes sign. Indeed, as can be seen from Eq. (26), g_1^n is larger than $g_{1\ \mathrm{exp}}^n$ for $x > x_0$, i.e., g_1^n changes sign at smaller x than $g_{1\ \mathrm{exp}}^n$. In order to see the magnitude of this effect, we analyze Eq. (26) with g_1^p and g_1^n given by the parametrization of Ref. [13]. Note that g_1^n obtained in Ref. [13] was fitted to the experimental data without the correction associated the Δ isobar and thus corresponds to $g_{1\ \mathrm{exp}}^n$. Figure 6 presents g_1^n based on Eq. (26) as a solid curve and the free neutron spin structure function $g_{1\ \mathrm{exp}}^n$ as a dashed curve. The two curves correspond to $Q^2 = 4\ \mathrm{GeV}^2$.

One can see from Fig. 6 that for a given choice of Q^2 and

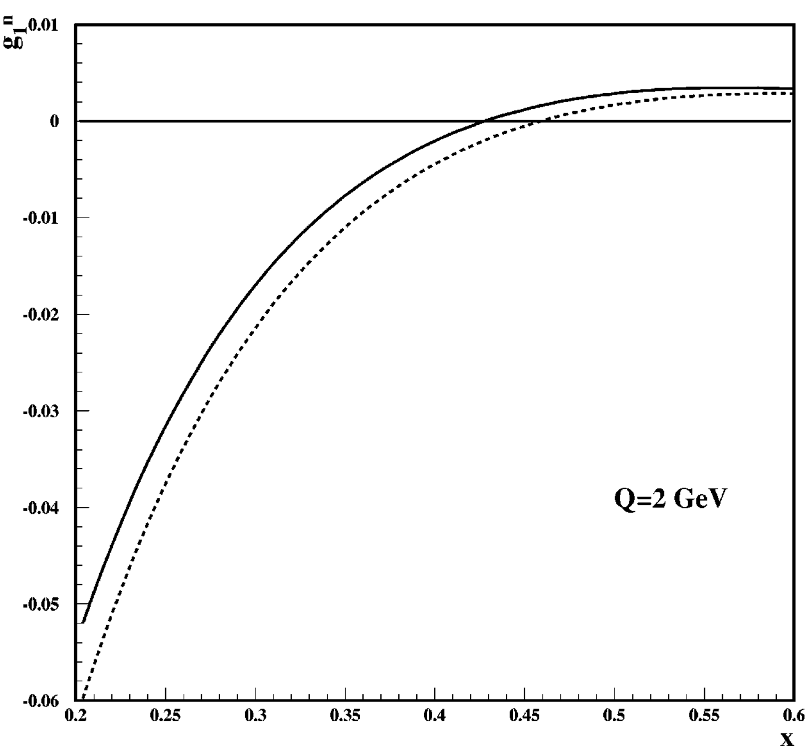

FIG. 6. The neutron spin structure function g_1^n based on Eq. (26) (solid curve) compared to the case based on the parametrization of Ref. [13] (dashed curve).

shapes of g_1^n and g_1^p, the presence of the Δ shifts the point where g_1^n changes sign, from 0.46 to 0.43.

The effect of the Δ on the ratio $g_1^n/g_{1\,\mathrm{exp}}^n$ is much more dramatic. If we formed the ratio $g_1^n/g_{1\,\mathrm{exp}}^n$ using the results presented in Fig. 6 (i.e., the ratio of the solid and dotted curves of Fig. 6), its shape would be quite similar to the tendency presented in Fig. 5: $g_1^n/g_{1\,\mathrm{exp}}^n$ dips below unity for $0.2 \leqslant x < 0.4$ and rises above unity for $x > 0.5$. However, the ratio $g_1^n/g_{1\,\mathrm{exp}}^n$ exhibits extremely rapid changes from being large and negative to large and positive in the interval $0.4 < x < 0.5$, where g_1^n changes sign. This effect is not seen in Fig. 5, where the discrete values of $g_{1\,\mathrm{exp}}^n$ are never close enough to zero. In the future, experimental studies of $g_{1\,\mathrm{exp}}^n$ near its zero would provide a very sensitive test of our model for the contribution of the Δ isobar to $g_1^{^3\mathrm{He}}$.

VI. A_1^n FROM THE ^{3}He DATA AT LARGE x

In this section we derive the expression necessary to extract the neutron asymmetry A_1^n from the ^{3}He data, which takes into account the presence of the Δ isobar in the ^{3}He wave function. This calculation is motivated by the E99-117 experiment that is currently under way at TJNAF (USA) [32]. Using DIS on polarized ^{3}He, the neutron asymmetry A_1^n will be extracted from the ^{3}He asymmetry $A_1^{^3\mathrm{He}}$, which is measured with high accuracy in the large-x region, $0.33 \leqslant x \leqslant 0.63$.

The DIS asymmetry A_1^T for any target T is proportional to the spin structure function of the target, g_1^T:

$$g_1^T = \frac{F_2^T}{2x(1+R)} A_1^T, \tag{27}$$

where $R = (F_2^T - 2xF_1^T)/(2xF_1^T)$ and $F_{1,2}^T$ are inclusive spin-averaged structure functions. It is assumed in Eq. (27) that the transverse spin asymmetry, A_2^n, is negligibly small and that R does not depend on the choice of target.

Applying this definition of A_1^T to ^{3}He, proton and neutron targets and substituting into Eq. (25), where the terms proportional to a and b were omitted (we are interested in the large x region, where shadowing and antishadowing are not present), one obtains, for the neutron asymmetry A_1^n,

$$A_1^n = \frac{F_2^{^3\mathrm{He}}}{P_n F_2^n\left(1 + \dfrac{0.056}{P_n}\right)} \times \left[A_1^{^3\mathrm{He}} - 2\frac{F_2^p}{F_2^{^3\mathrm{He}}} P_p A_1^p \left(1 - \frac{0.014}{2P_p}\right)\right]. \tag{28}$$

Provided that the proton asymmetry A_1^p is constrained well by the experimental data, the largest theoretical uncertainty (which is of the order 10%) in Eq. (28) comes from the uncertainty in the proton spin polarization P_p. Thus we estimate that the uncertainty in the second term of Eq. (28) and thus in the position of the point where A_1^n has a zero, is of the order 10%.

The terms proportional to 0.056 and 0.014 represent the correction to A_1^n associated with the Δ isobar. Both terms are important for the correct determination of A_1^n. The term proportional to 0.056 decreases the absolute value of A_1^n by about 6%. Moreover, if $A_1^{^3\mathrm{He}}$ is negative, the second term proportional to 0.014 would work in the same direction of decreasing of $|A_1^{^3\mathrm{He}}|$. Since the term proportional to 0.014 is always positive, this means that the true A_1^n should turn positive at lower values of x compared to the situation when the effect of the Δ is ignored (see Fig. 6).

VII. SUMMARY AND CONCLUSIONS

We presented a comprehensive picture of nuclear effects relevant for DIS on polarized ^{3}He, over a wide range of Bjorken x, $10^{-4} \leqslant x \leqslant 0.8$. These effects include nuclear shadowing and antishadowing, nucleon spin depolarization, Fermi motion and binding, the presence of the Δ isobar in the ^{3}He wave function, and the off-shellness of the nucleons. For the first time, all the above effects were studied in a uniform fashion using the ground-state wave function of ^{3}He, which was obtained as a solution of the Faddeev equation with a separable version of the Paris nucleon-nucleon potential (PEST) with five channels. It is crucial to include all relevant nuclear effects for the proper determination of the neutron spin structure function g_1^n from the ^{3}He data. In particular, we emphasized that the commonly used approximate expression for $g_1^{^3\mathrm{He}}$ based on Eq. (2) receives important corrections from the effects associated with nuclear shadowing and antishadowing and the Δ isobar [see Eq. (25)]. As a consequence, the values of the neutron spin structure function g_1^n deduced from the ^{3}He data by the E154 experiment at SLAC and the HERMES experiment at DESY should be corrected. Our results should be also taken into consideration in analysing the results of future DIS experiments on polarized ^{3}He, such as, for instance, the E99-117 experiment at TJNAF. Our results are summarized below, starting from the smallest x.

At small values of Bjorken x, $10^{-4} \leqslant x \leqslant 0.2$, $g_1^{^3\mathrm{He}}$ is affected by nuclear shadowing and antishadowing as well as nucleon spin depolarization effects [see Eq. (23)]. As a result, the deviation from the approximate expression for $g_1^{^3\mathrm{He}}$ given by Eq. (2) could be as large as 8% at $x = 10^{-3}$. This requires a 4% decrease of the lowest-x values for g_1^n reported by the E154 and HERMES experiments. The effect of the antishadowing correction to $g_1^{^3\mathrm{He}}$ is somewhat smaller and works in the opposite direction: the experimental values for the extracted g_1^n should be increased. For instance, the increase is 7% at $x = 0.13$. Note, however, that our treatment of antishadowing is model dependent and our predictions for the amount of antishadowing (and shadowing at x close to x_0) depend crucially on the choice of x_0, the crossover point between the nuclear shadowing and antishadowing regions.

At larger x, $0.2\leqslant x\leqslant 0.8$, the three principal nuclear effects are the nucleon spin depolarization, the presence of the $\Delta(1232)$ resonance in the ^{3}He wave function, and Fermi motion and binding effects. The effect of the Δ works to decrease $g_1^{^3\mathrm{He}}$. For example, the decrease is of the order 12% at $x=0.2$. The modification caused by the Δ is very significant at $x\approx 0.46$, where g_1^n (in the particular parametrization of Ref. [13]) is expected to change sign (for example, predictions for the shape of g_1^n were derived in Ref. [33] within the MIT bag model). In the region $0.2\leqslant x\leqslant 0.8$, the E154 and HERMES values for g_1^n should be increased by as much as 15–25%. Also, the effect associated with the Δ is expected to increase the neutron DIS asymmetry A_1^n, which will be measured by the E99-117 experiment at TJNAF. As a result, the true g_1^n should change sign at lower x.

The data files with the results presented in this work are available on request from V. Guzey.

ACKNOWLEDGMENTS

We would like to thank K. Tsushima for discussions concerning the results of Ref. [11] and Z.-E. Meziani for raising the question of the extraction of A_1^n from $A_1^{^3\mathrm{He}}$ related to the 99-117 experiment at TJNAF. This work was supported by the Australian Research Council, Adelaide University, and the U.S. Department of Energy.

APPENDIX: NUCLEAR SHADOWING IN POLARIZED DIS ON ^{3}He

In order to estimate nuclear shadowing in polarized DIS on ^{3}He we use the standard Gribov-Glauber multiple scattering formalism (for a pedagogical review of the method, see Ref. [34]). The cross section for h_{eff}-^{3}He scattering [see Eqs. (19),(20),(21)] with parallel helicities, $\sigma^{\uparrow\uparrow}_{h_{\mathrm{eff}}{}^3\mathrm{He}}$, can be expressed through the nuclear profile function $\Gamma^{\uparrow\uparrow}_{^3\mathrm{He}}$:

$$\sigma^{\uparrow\uparrow}_{h_{\mathrm{eff}}{}^3\mathrm{He}}=2\,\mathrm{Re}\int d^2b\,\Gamma^{\uparrow\uparrow}_{^3\mathrm{He}}(b), \tag{A1}$$

where $\vec{b}$ is a vector of the impact parameter, the distance between the projectile and the center of the nucleus in the plane transverse to the direction of the projectile. The nuclear profile function $\Gamma^{\uparrow\uparrow}_{^3\mathrm{He}}$ is obtained as a series over nucleon spin-dependent profile functions $\Gamma_i(\vec{b}-\vec{r}_{i\perp})$ averaged with the ground-state wave function of ^{3}He,

$$\begin{aligned}\Gamma^{\uparrow\uparrow}_{^3\mathrm{He}}=&\langle\Psi^{\uparrow}_{^3\mathrm{He}}|\sum_i^3\sum_s\Gamma_i^{\uparrow s}(\vec{b}-\vec{r}_{i\perp})-\sum_{i\neq j}^3\sum_{s_1,s_2}\Gamma_i^{\uparrow s_1}\\&\times(\vec{b}-\vec{r}_{i\perp})\Gamma_j^{\uparrow s_2}(\vec{b}-\vec{r}_{j\perp})\Theta(z_j-z_i)e^{iq_{\parallel}(z_i-z_j)}\\&+\sum_{i\neq j\neq k}^3\sum_{s_1,s_2,s_3}\Gamma_i^{\uparrow s_1}(\vec{b}-\vec{r}_{i\perp})\Gamma_j^{\uparrow s_2}(\vec{b}-\vec{r}_{j\perp})\\&\times\Gamma_k^{\uparrow s_3}(\vec{b}-\vec{r}_{k\perp})\Theta(z_j-z_i)\Theta(z_k-z_j)\\&\times e^{iq_{\parallel}(z_i-z_k)}|\Psi^{\uparrow}_{^3\mathrm{He}}\rangle.\end{aligned} \tag{A2}$$

The helicity of the virtual photon is denoted by the first arrow in the superscripts; the helicity of the target nucleus is shown by an arrow next to the nuclear wave function. Since the helicities of the nucleons need not be aligned with the helicity of the target, there are sums over helicities of the nucleons (symbolized by s_1, s_2, and s_3 in the superscripts). The subscripts on the Γ's (i, j, and k) are designed to distinguish between the neutrons and protons. Positions of the nucleons with respect to the center of the nucleus are given by transverse ($\vec{r}_{i\perp}$) and longitudinal (z_i) coordinates. The factors $e^{iq_{\parallel}(z_i-z_j)}$ take into account the nonzero longitudinal momentum transferred to the nucleus, $q_{\parallel}\approx 2m_N x$, where m_N is the nucleon mass.

Using time reversal one can show that the Θ functions in the double scattering terms of Eq. (A2) can be substituted by 1/2 and that the product of two Θ functions in the triple scattering term can be substituted by 1/6. In addition, choosing the normalization of the ^{3}He wave function such that, for example, the first nucleon is the neutron (with coordinates $\vec{r}_n$) and the other two are protons (with coordinates $\vec{r}_p$ and $\vec{r}_{p'}$), Eq. (A2) can be presented in the form

$$\begin{aligned}\Gamma^{\uparrow\uparrow}_{^3\mathrm{He}}=&\langle\Psi^{\uparrow}_{^3\mathrm{He}}|\sum_s[\Gamma_n^{\uparrow s}(\vec{b}-\vec{r}_{n\perp})+2\Gamma_p^{\uparrow s}(\vec{b}-\vec{r}_{p\perp})]\\&-\sum_{s_1,s_2}[2\Gamma_n^{\uparrow s_1}(\vec{b}-\vec{r}_{n\perp})\Gamma_p^{\uparrow s_2}(\vec{b}-\vec{r}_{p\perp})e^{iq_{\parallel}(z_n-z_p)}\\&+\Gamma_p^{\uparrow s_1}(\vec{b}-\vec{r}_{p\perp})\Gamma_p^{\uparrow s_2}(\vec{b}-\vec{r}_{p'\perp})e^{iq_{\parallel}(z_p-z_{p'})}]\\&+\sum_{s_1,s_2,s_3}\Gamma_n^{\uparrow s_1}(\vec{b}-\vec{r}_{n\perp})\\&\times\Gamma_p^{\uparrow s_2}(\vec{b}-\vec{r}_{p\perp})\Gamma_p^{\uparrow s_3}(\vec{b}-\vec{r}_{p'\perp})e^{iq_{\parallel}(z_n-z_{p'})}|\Psi^{\uparrow}_{^3\mathrm{He}}\rangle.\end{aligned} \tag{A3}$$

Each spin-dependent nucleon profile function is related to the spin-dependent h_{eff}-nucleon scattering cross section $\sigma_N^{\uparrow s}$ and the slope B (whose value is discussed later):

$$\Gamma_{n,p}^{\uparrow s}(\vec{r}_\perp)=\frac{\sigma_{n,p}^{\uparrow s}}{4\pi B}e^{-\vec{r}_\perp^{\,2}/(2B)}. \tag{A4}$$

Combining Eqs. (A1),(A3),(A4) one obtains for the h_{eff}-^{3}He spin-dependent scattering cross section

$$\begin{aligned}\sigma^{\uparrow\uparrow}_{h_{\mathrm{eff}}{}^3\mathrm{He}}=&\langle\Psi^{\uparrow}_{^3\mathrm{He}}|\sum_s(\sigma_n^{\uparrow s}\hat{P}_n^s+2\sigma_p^{\uparrow s}\hat{P}_p^s)\\&-\frac{1}{8\pi B}\sum_{s_1,s_2}(2\sigma_n^{\uparrow s_1}\sigma_p^{\uparrow s_2}\hat{P}_{np}^{s_1s_2}+\sigma_p^{\uparrow s_1}\sigma_p^{\uparrow s_2}\hat{P}_{pp}^{s_1s_2})\\&+\frac{1}{48\pi^2B^2}\sum_{s_1,s_2,s_3}\sigma_n^{\uparrow s_1}\sigma_p^{\uparrow s_2}\sigma_p^{\uparrow s_3}\hat{P}_{npp}^{s_1s_2s_3}|\Psi^{\uparrow}_{^3\mathrm{He}}\rangle.\end{aligned} \tag{A5}$$

Here the $\hat{P}$'s are projection operators onto one or several nucleons of ^{3}He with particular helicities. The cross section for $h_{\rm eff}$-^{3}He scattering with antiparallel helicities $\sigma^{\uparrow\downarrow}_{h_{\rm eff}{}^3{\rm He}}$ is obtained from Eq. (A5) by inverting the helicity of the target.

Next we introduce cross sections $\Delta\sigma$ and $\sigma_{\rm eff}$,

$$\sigma^{\uparrow\uparrow}_{n,p}\equiv\sigma_{\rm eff}+\frac{1}{2}\Delta\sigma_{n,p},$$

$$\sigma^{\uparrow\downarrow}_{n,p}\equiv\sigma_{\rm eff}-\frac{1}{2}\Delta\sigma_{n,p}. \tag{A6}$$

Here we do not distinguish between the spin-averaged cross sections for protons and neutrons, i.e., $\sigma_{\rm eff}$ is the same for the interaction with protons and neutrons.

Using Eqs. (A5),(A6) the difference between the $h_{\rm eff}$-^{3}He scattering cross sections with parallel and antiparallel helicities, $\Delta\sigma_{h_{\rm eff}{}^3{\rm He}}$, can be presented in the form

$$\Delta\sigma_{h_{\rm eff}{}^3{\rm He}}\equiv\sigma^{\uparrow\uparrow}_{h_{\rm eff}A}-\sigma^{\uparrow\downarrow}_{h_{\rm eff}A}$$
$$=P_n\Delta\sigma_n+2P_p\Delta\sigma_p-\frac{\sigma_{\rm eff}}{4\pi B}(\Delta\sigma_n\Phi_n+\Delta\sigma_p\Phi_p)$$
$$+\frac{\sigma^2_{\rm eff}}{48\pi^2(\alpha_{^3{\rm He}}+B)^2}\Delta\sigma_n. \tag{A7}$$

Several remarks concerning Eq. (A7) are in order here. First, P_n and P_p are effective proton and neutron spin polarizations defined by Eq. (3). We use $P_n=0.879$ and $P_p=-0.021$. Second, the nuclear shadowing correction to $\Delta\sigma_{h_{\rm eff}A}$, which is given by the third and fourth terms of Eq. (A7), is determined by the effective spin-averaged cross section $\sigma_{\rm eff}$. This cross section defines the strength of the interaction with a pair of nucleons of the nuclear target, which determines the size of nuclear shadowing. The shape of $\sigma_{\rm eff}$ as a function of x at $Q^2=4$ GeV^2 is shown in Fig. 2 of Ref. [28] (note that we modified $\sigma_{\rm eff}$ for $x>0.01$ so that it vanishes at $x_0=0.03$ or $x_0=0.07$). For instance, $\sigma_{\rm eff}\approx 15$ mb at $x=10^{-3}$. As discussed in Sec. IV, we made an assumption that $\sigma_{\rm eff}$ is the same as the effective cross section for sea quarks, which was determined in the analysis of unpolarized DIS on nuclei within the framework on the approach [28]. This means that we assume that the strenghs of nuclear shadowing in inpolarized and polarized DIS on nuclei are the same. Third, the nuclear shadowing correction due to triple scattering, given by the last term in Eq. (A7), is small. As discussed in Sec. IV, our numerical analysis demonstrated that the calculations with the exact (including higher partial waves) and highly simplified (where only the neutron is polarized) wave functions of ^{3}He give very close results for the nuclear shadowing correction. Thus, to estimate the triple scattering contribution, it is safe to use a simple Gaussian ansatz for the ^{3}He ground-state wave function with $\alpha_{^3{\rm He}}=27$ GeV^{-2} and assume that only the neutron is polarized [17]. Fourth, the main effect of nuclear shadowing comes from the double scattering terms (proportional to Φ_n and Φ_p) which need to be carefully evaluated.

The functions Φ_n and Φ_p are defined as

$$\Phi_n=\sum_{s_1,s_2}\int\prod_i d^3\vec{r}_i[|\Psi^{\uparrow}_{^3{\rm He}}(\vec{r}_n,\uparrow;\vec{r}_p,s_1;\vec{r}_{p'},s_2)|^2$$
$$-|\Psi^{\uparrow}_{^3{\rm He}}(\vec{r}_n,\downarrow;\vec{r}_p,s_1;\vec{r}_{p'},s_2)|^2]$$
$$\times e^{-(\vec{r}_{n\perp}-\vec{r}_{p\perp})^2/(4B)}\cos q_{\parallel}(z_n-z_p),$$

$$\Phi_p=\sum_{s_1,s_2}\int\prod_i d^3\vec{r}_i[|\Psi^{\uparrow}_{^3{\rm He}}(\vec{r}_n,s_1;\vec{r}_p,\uparrow;\vec{r}_{p'},s_2)|^2$$
$$-|\Psi^{\uparrow}_{^3{\rm He}}(\vec{r}_n,s_1;\vec{r}_p,\uparrow;\vec{r}_{p'},s_2)|^2]$$
$$\times e^{-(\vec{r}_{n\perp}-\vec{r}_{p\perp})^2/(4B)}\cos q_{\parallel}(z_n-z_p)$$
$$+\sum_{s}\int\prod_i d^3\vec{r}_i[|\Psi^{\uparrow}_{^3{\rm He}}(\vec{r}_n,s;\vec{r}_p,\uparrow;\vec{r}_{p'},\uparrow)|^2$$
$$-|\Psi^{\uparrow}_{^3{\rm He}}(\vec{r}_n,s;\vec{r}_p,\downarrow;\vec{r}_{p'},\downarrow)|^2]$$
$$\times e^{-(\vec{r}_{p\perp}-\vec{r}_{p'\perp})^2/(4B)}\cos q_{\parallel}(z_p-z_{p'}). \tag{A8}$$

Here $B=6$ GeV^{-2} is the slope of the elementary $h_{\rm eff}$-nucleon scattering cross section. The used value for the slope B requires discussion. It should be noted that, within the framework of Ref. [28], the elementary $h_{\rm eff}$-nucleon scattering cross section is proportional to the diffractive electron-proton DIS cross section. Thus B is in fact the slope of the diffractive electron-proton DIS cross section. The ZEUS Collaboration measurement gives $B=7.2\pm1.1$ GeV^{-2} [35] in the HERA kinematics. Since B decreases slowly with decreasing energy, a slightly smaller value for B, $B=6$ GeV^{-2}, seems to be more appropriate for the kinematics of fixed target experiments on polarized DIS on nuclear targets.

For the ground-state wave function of ^{3}He we used the one obtained by solving the Faddeev equations with the PEST two-nucleon interaction potential including five channels [9].

Using the relation between the spin structure function $g_1^{^3{\rm He}}$ and the difference of the cross sections, $\Delta\sigma_{h_{\rm eff}{}^3{\rm He}}$ [see Eq. (21)], one can find the most complete expression for the ^{3}He spin structure function $g_1^{^3{\rm He}}$ [see Eqs. (22),(23)],

$$g_1^{^3{\rm He}}=\int_x^3\frac{dy}{y}\Delta f_{n/^3{\rm He}}(y)\tilde{g}_1^n(x/y)$$
$$+\int_x^3\frac{dy}{y}\Delta f_{p/^3{\rm He}}(y)\tilde{g}_1^p(x/y)-0.014[\tilde{g}_1^p(x)-4\tilde{g}_1^n(x)]$$
$$+a^{sh}(x)g_1^n(x)+b^{sh}(x)g_1^p(x), \tag{A9}$$

where

$$a^{sh}(x,Q^2)=-\frac{\sigma_{\rm eff}}{4\pi B}\Phi_n+\frac{\sigma_{\rm eff}^2}{48\pi^2(\alpha_{^3{\rm He}}+B)^2}$$

$$b^{sh}(x,Q^2)=-\frac{\sigma_{\rm eff}}{4\pi B}\Phi_p\,. \tag{A10}$$

In Eq. (A9), we replaced the single scattering terms proportional to P_n and P_n by their generalization in terms of the convolution with the off-shell nucleon structure functions. Also, the effects associated with the presence of the Δ isobar were included.

[1] SMC Collaboration, B. Adeva *et al.*, Phys. Lett. B **302**, 533 (1993); D. Adams *et al.*, *ibid.* **357**, 248 (1995); **396**, 338 (1997); B. Adeva *et al.*, Phys. Rev. D **58**, 112001 (1998).

[2] E143 Collaboration, K. Abe *et al.*, Phys. Lett. B **364**, 61 (1995); K. Abe *et al.*, Phys. Rev. Lett. **75**, 25 (1995); Phys. Rev. D **58**, 112003 (1998).

[3] E155 Collaboration, P. L. Anthony *et al.*, Phys. Lett. B **463**, 339 (1999); P. L. Anthony *et al.*, *ibid.* **493**, 19 (2000).

[4] HERMES Collaboration, K. Ackerstaff *et al.*, Phys. Lett. B **404**, 383 (1997).

[5] E154 Collaboration, K. Abe *et al.*, Phys. Lett. B **404**, 377 (1997); K. Abe *et al.*, *ibid.* **405**, 180 (1997); Phys. Rev. Lett. **79**, 26 (1997).

[6] R. L. Jaffe, in *Relativistic Dynamics and Quark-Nuclear Physics*, edited by M. B. Johnson and A. Picklesiner (Wiley, New York, 1986).

[7] C. Ciofi degli Atti, S. Scopetta, E. Pace, and G. Salme, Phys. Rev. C **48**, R968 (1993).

[8] R.-W. Schulze and P. U. Sauer, Phys. Rev. C **48**, 38 (1993).

[9] F. Bissey, A. W. Thomas, and I. R. Afnan, Phys. Rev. C **64**, 024004 (2001).

[10] J. L. Friar, B. F. Gibson, G. L. Payne, A. M. Bernstein, and T. E. Chupp, Phys. Rev. C **42**, 2310 (1990).

[11] F. M. Steffens, K. Tsushima, A. W. Thomas, and K. Saito, Phys. Lett. B **447**, 233 (1999).

[12] P. A. M. Guichon, Phys. Lett. B **200**, 235 (1988); P. A. M. Guichon, K. Saito, E. Rodionov, and A. W. Thomas, Nucl. Phys. **A601**, 349 (1996).

[13] M. Gluck, E. Reya, M. Stratmann, and W. Wogelsang, Phys. Rev. D **63**, 094005 (2001).

[14] I. R. Afnan *et al.*, Phys. Lett. B **493**, 36 (2000).

[15] M. M. Sargsian, S. Simula, and M. I. Strikman, nucl-th/0105052.

[16] G. Piller, W. Melnitchouk, and A. W. Thomas, Phys. Rev. C **54**, 894 (1996).

[17] L. Frankfurt, V. Guzey, and M. Strikman, Phys. Lett. B **381**, 379 (1996).

[18] J. D. Bjorken, Phys. Rev. **148**, 1467 (1966).

[19] Particle Data Group, C. Caso *et al.*, Eur. Phys. J. C **3**, 1 (1998).

[20] B. Budick, Jiansheng Chen, and Hong Lin, Phys. Rev. Lett. **67**, 2630 (1991).

[21] T.-Y. Saito Y. Wu, S. Ishikawa, and T. Sasakawa, Phys. Lett. B **242**, 12 (1990); J. Carlson, D. Riska, R. Schiavilla, and R. B. Wiringa, Phys. Rev. C **44**, 619 (1991).

[22] C. Boros, V. Guzey, M. Strikman, and A. W. Thomas, Phys. Rev. D **64**, 014025 (2001).

[23] F. E. Close and A. W. Thomas, Phys. Lett. B **212**, 227 (1988); C. Boros and A. W. Thomas, Phys. Rev. D **60**, 074017 (1999).

[24] NMC Collaboration, P. Amaudruz *et al.*, Nucl. Phys. **B441**, 3 (1995); M. Arneodo *et al.*, *ibid.* **B441**, 12 (1995).

[25] J. Edelmann, G. Piller, and W. Wiese, Z. Phys. A **357**, 129 (1997); Phys. Rev. C **57**, 3392 (1998).

[26] V. Guzey and M. Strikman, Phys. Rev. C **61**, 014002 (1999).

[27] V. Guzey, Phys. Rev. C **64**, 045201 (2001).

[28] L. Frankfurt and M. Strikman, Eur. Phys. J. A **5**, 293 (1999).

[29] W. Melnitchouk and A. W. Thomas, Phys. Lett. B **317**, 437 (1993); Phys. Rev. C **52**, 3373 (1995); J. Kwiecinski and B. Badelek, Phys. Lett. B **208**, 508 (1988).

[30] S. J. Brodsky and H. J. Lu, Phys. Rev. Lett. **64**, 1342 (1990).

[31] W. Melnitchouk and A. W. Thomas, Phys. Rev. D **47**, 3783 (1993). The original publications on the subject include C. H. Llewellyn Smith, Phys. Lett. **128B**, 107 (1983); M. Ericson and A. W. Thomas *ibid.* **128B**, 112 (1983).

[32] Proposal of the E-99-117 experiment at TJNAF "Precision measurement of the neutron asymmetry A_1^n at large x_{Bj} using TJNAF at 6 GeV," Z.-E. Meziani, J.-P. Chen, and P. Souder, spokepersons.

[33] A. W. Schreiber, A. I. Signal, and A. W. Thomas, Phys. Rev. D **44**, 2653 (1991); F. M. Steffens, H. Holtmann, and A. W. Thomas, Phys. Lett. B **358**, 139 (1995).

[34] T. H. Bauer, R. D. Spital, and D. R. Yennie, Rev. Mod. Phys. **50**, 261 (1978); **51**, 407(E) (1979).

[35] ZEUS Collaboration, Eur. Phys. J. C **1**, 81 (1998).